Geomechanics and Engineering, *Vol. 29, No. 1 (2022) 53-63*
https://doi.org/10.12989/gae.2022.29.1.053

Dynamic analyses for an axially-loaded pile in a transverse-isotropic, fluid-filled, poro-visco-elastic soil underlain by rigid base

Shiping Zhang[1,2], Junhui Zhang*[1,2], Ling Zeng[3], Cheng Yu[4] and Yun Zheng[5]

[1]*Key Laboratory of Road Structure and Material of Ministry of Transport (Changsha), China*
[2]*School of Traffic and Transportation Engineering, Changsha University of Science & Technology, Changsha 410114, Hunan, China*
[3]*School of Civil Engineering, Changsha University of Science & Technology, Changsha 410114, Hunan, China*
[4]*Dalian Bohai detection Co., Ltd, Dalian 116031, Liaoning, China*
[5]*Institute of Rock and Soil Mechanics, Chinese Academy of Sciences, Wuhan 430071, China*

(Received October 16, 2019, Revised February 11, 2022, Accepted February 15, 2022)

Abstract. Simplified analytical solutions are developed for the dynamic analyses of an axially loaded pile foundation embedded in a transverse-isotropic, fluid-filled, poro-visco-elastic soil with rigid substratum. The pile is modeled as a viscoelastic Rayleigh-Love rod, while the surrounding soil is regarded as a transversely isotropic, liquid-saturated, viscoelastic, porous medium of which the mechanical behavior is represented by the Boer's poroelastic media model and the fractional derivative model. Upon the separation of variables, the frequency-domain responses for the impedance function of the pile top, and the vertical displacement and the axial force along the pile shaft are gained. Then by virtue of the convolution theorem and the inverse Fourier transform, the time-domain velocity response of the pile head is derived. The presented solutions are validated, compared to the existing solution, the finite element model (FEM) results, and the field test data. Parametric analyses are made to show the effect of the soil anisotropy and the excitation frequency on the pile-soil dynamic responses.

Keywords: Boer's poroelastic model; pile; transversely isotropic; poro-visco-elastic; separation of variables

1. Introduction

Dynamic responses of pile foundations and the surrounding soils have been of essential significance in structural, seismic, and geotechnical engineering (e.g., Barari *et al*. 2015, Cui *et al*. 2018, Zhang *et al*. 2021). In general, by regarding the piles as beams while the surrounding soils as elastic continuum, the dynamic responses of the pile-soil systems can be obtained by solving their governing equations and imposing the pile-soil boundary and continuity conditions (e.g., Zhang *et al*. 2022). Since Tajimi (1969) presented the dynamic analysis of a structure embedded in an elastic stratum, by following the pioneering work comprehensive researches for the dynamic

responses of the piles and soils of isotropic elastic materials have been conducted in classical treatments (e.g., Nogami and Novak 1976, Novak 1977).

Due to the long-term sedimentation or consolidation process, soil materials, however, are usually anisotropic and instead have significant property difference in the vertical and horizontal directions, which is characterized by the transverse isotropy in their mechanical properties (e.g., Wang and Liao 2001, Wang 2004). To take into account the effect of the soil anisotropic property on the pile-soil interaction, by employing the transversely isotropic constitutive relationship to describe the soil, Shahmohamadi *et al*. (2011a, b, 2013), Gharahi *et al*. (2014), Ai and Li (2015), Ai and Liu (2015), Ai *et al*. (2016a, b), Shahbodagh *et al*. (2017), Barros *et al*. (2019) investigated the dynamic responses for the piles buried in transverse-isotropic, single-phase, semi-infinite half-spaces under vertical, horizontal loads, or P-wave excitations. While by considering the surrounding soils as transversely isotropic, liquid-saturated half-spaces or soil layers with finite thickness, Chen *et al.* (2008), Wang *et al*. (2009), Zheng *et al*. (2016), Zhang *et al*. (2019) studied the dynamic responses for the embedded piles subjected to torsional or vertical loads.

As can be found from the above-mentioned studies, the soils are generally viewed as purely elastic semi-infinite half-spaces, and therefore the effects of the pore liquid in the soils and the wave reflection disturbance from the underlain bedrock are seldom considered. As we know, natural soils can be fluid-filled porous media, especially in coastal regions and meanwhile may rest on hard rocks in many cases (e.g., Zhang *et al.* 2021, Zhang *et al.* 2022). Thus, studying the dynamic characteristic of the piles in such soils is important in developing guidelines for related engineering applications. However, so far the researches about the dynamic analyses for piles embedded in transverse-isotropic, porous media resting on rigid bedrock have been rarely reported.

In light of the above, this paper aims to propose the dynamic analyses for axially loaded piles buried in transverse-isotropic, poro-visco-elastic soils resting on rigid base with analytical investigation. The pile is modeled as a viscoelastic Rayleigh-Love rod with the beam vibration

*Corresponding author, Professor
E-mail: zjhseu@126.com

ISSN: 2005-307X (Print), 2092-6219 (Online)

theory. While the surrounding soil is regarded as a transversely isotropic, fluid-filled, viscoelastic, porous medium, of which the mechanical behavior is represented by the Boer's poroelastic media model and the fractional derivative model. By employing the variables separation theory to deal with the soil governing equations, the soil reaction on the pile side surface is derived. Furthermore, using the derived soil reaction, the dynamic governing equation of the embedded pile is built. Then by resolving the pile governing equation and imposing the pile-soil boundary and compatibility conditions, the frequency-domain analytical solutions for the impedance function at the pile head, and the pile's displacement and axial force are obtained. By virtue of the convolution theorem and the inverse Fourier transform, the time-domain velocity response at the pile head is gained from the frequency-domain pile displacement solution. The presented solutions are validated, compared to the reported solution, the FEM results, and the field test data. Finally, parametric analyses for numerical examples are conducted to show the influence of the soil anisotropy and the excitation frequency on the pile-soil dynamic responses.

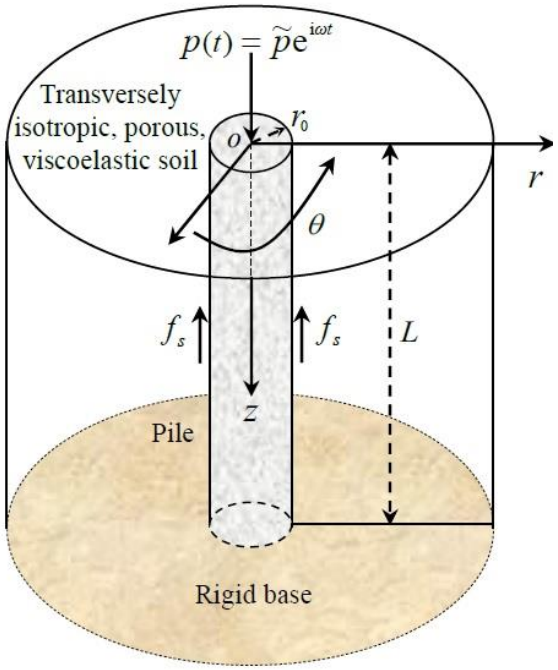

Fig. 1 An axially-loaded pile embedment in a transverse-isotropic, fluid-filled, poro-visco-elastic soil underlain by rigid base

2. Problem statement and resolving

As Fig. 1 pictures, in the cylindrical-coordinate system a viscoelastic rod of length L and radius r_0 is entirely buried in a transversely isotropic, liquid-filled, poro-visco-elastic subsoil overlaying rigid base. A time-harmonic loading of $p(t)=\tilde{p}e^{i\omega t}$ ($i=\sqrt{-1}$, and $\omega=2\pi f$ denotes the circular frequency) is vertically applied at the rod top center of ($r=0, \theta, z=0$).

Also, the fundamental assumptions of the pile-soil system are prescribed as following:

·The constitutive relationships for the pile and the soil are linearly elastic;

·Infinitesimal deformations for the pile-soil system;

·During vibration the pile-soil interfaces are fully bonded, and then no pile-soil relative sliding and separation.

2.1 Governing equations for the soil and the pile

Using the Boer's porous media model (1994) to describe the saturated soil, of which the momentum and mass balance equations can be written by

$$\nabla\cdot\boldsymbol{\sigma}^s - n^s\nabla p^f + \boldsymbol{S}_v(\dot{\boldsymbol{u}}_f - \dot{\boldsymbol{u}}_s) - \rho^s\ddot{\boldsymbol{u}}_s = 0 \tag{1a}$$

$$-n^f\nabla p^f - \boldsymbol{S}_v(\dot{\boldsymbol{u}}_f - \dot{\boldsymbol{u}}_s) - \rho^f\ddot{\boldsymbol{u}}_f = 0 \tag{1b}$$

$$\nabla\cdot(n^s\dot{\boldsymbol{u}}_s + n^f\dot{\boldsymbol{u}}_f) = 0 \tag{1c}$$

where $\boldsymbol{\sigma}^s$ denotes the effective stress tensor for the soil skeleton while p^f the pore fluid pressure. n^s and n^f are respectively the volume fractions for the soil granule and the pore fluid, and $n^s + n^f = 1$ for the complete saturation condition. $\boldsymbol{S}_v$ represents the coefficient tensor describing the liquid-solid interplay. $\rho^s = n^s\rho^{sR}$ and $\rho^f = n^f\rho^{fR}$ respectively express the volume densities for the soil granule and the pore fluid. $\boldsymbol{u}_s$ and $\boldsymbol{u}_f$ respectively denote the displacement vectors for the soil granule and the pore fluid. Dots over displacement vectors indicate the derivatives versus the time variable of t. ∇ is the gradient operator.

The pile-soil system pictured in Fig. 1 is axisymmetrical about z-axis, so all field variables are independent about θ and the circumferential displacement of the soil vanishes. Using the fraction derivative model by Bagley and Torvik (1983) and the transversely isotropic constitutive model to respectively describe the viscosity and anisotropy for the soil skeleton, the linear stress-displacement relationship for the soil skeleton can be denoted in the component terms of

$$(1+\tau_\varepsilon^\alpha D^\alpha)\sigma_{rr} = (1+\tau_\sigma^\alpha D^\alpha)(d_{11}\frac{\partial u_s}{\partial r} + d_{12}\frac{u_s}{r} + d_{13}\frac{\partial w_s}{\partial z}) \tag{2a}$$

$$(1+\tau_\varepsilon^\alpha D^\alpha)\sigma_{\theta\theta} = (1+\tau_\sigma^\alpha D^\alpha)(d_{12}\frac{\partial u_s}{\partial r} + d_{11}\frac{u_s}{r} + d_{13}\frac{\partial w_s}{\partial z}) \tag{2b}$$

$$(1+\tau_\varepsilon^\alpha D^\alpha)\sigma_{zz} = (1+\tau_\sigma^\alpha D^\alpha)(d_{13}\frac{\partial u_s}{\partial r} + d_{13}\frac{u_s}{r} + d_{33}\frac{\partial w_s}{\partial z}) \tag{2c}$$

$$(1+\tau_\varepsilon^\alpha D^\alpha)\tau_{zr} = (1+\tau_\sigma^\alpha D^\alpha)(d_{66}\frac{\partial w_s}{\partial r} + d_{66}\frac{\partial u_s}{\partial z}) \tag{2d}$$

where $d_{11}=\dfrac{E_{hs}(1-\upsilon_{hvs}\upsilon_{vhs})}{(1+\upsilon_{hhs})(1-\upsilon_{hhs}-2\upsilon_{hvs}\upsilon_{vhs})}$,

$d_{12}=\dfrac{E_{hs}(\upsilon_{hhs}+\upsilon_{hvs}\upsilon_{vhs})}{(1+\upsilon_{hhs})(1-\upsilon_{hhs}-2\upsilon_{hvs}\upsilon_{vhs})}$,

$d_{13}=\dfrac{E_{hs}\upsilon_{hhs}}{1-\upsilon_{hhs}-2\upsilon_{hvs}\upsilon_{vhs}}$, $d_{33}=\dfrac{E_{vs}(1-\upsilon_{hhs})}{1-\upsilon_{hhs}-2\upsilon_{hvs}\upsilon_{vhs}}$, and $d_{66}=G_{vs}$. Here, E_{hs} and E_{vs} respectively express the horizontal and vertical elasticity moduli. υ_{hvs} is the Poisson's ratio of the vertical strain generated from horizontal stresses, while υ_{vhs} that of the horizontal strain due to vertical stresses, and $\dfrac{\upsilon_{vhs}}{E_{vs}}=\dfrac{\upsilon_{hvs}}{E_{hs}}$. Also, υ_{hhs} denotes the Poisson's ratio for the orthogonally-horizontal strain generated from horizontal stresses. G_{vs} is the shearing modulus of the vertical plane. τ_ε and τ_σ are the parameters representing the soil viscosity. $D^\alpha=\dfrac{\mathrm{d}^\alpha}{\mathrm{d}t^\alpha}$, denoting the Riemann-Liouville's fraction derivative with the α order ($0<\alpha<1$) by Miller and Ross (1993), can be written as

$$D^\alpha[x(t)]=\frac{1}{\Gamma(1-\alpha)}\frac{\mathrm{d}}{\mathrm{d}t}\int_0^t\frac{x(\tau)}{(t-\tau)^\alpha}\mathrm{d}\tau \tag{3}$$

where $\Gamma(u)=\int_0^\infty t^{u-1}\mathrm{e}^{-u}\mathrm{d}t$ is the Gamma function.

By combining Eq. (1) through (3), the governing equations of the saturated soil are deduced as

$$(1+\tau_\sigma^\alpha D^\alpha)\begin{bmatrix}d_{11}(\frac{\partial^2 u_s}{\partial r^2}+\frac{1}{r}\frac{\partial u_s}{\partial r}-\frac{u_s}{r^2})+d_{66}\frac{\partial^2 u_s}{\partial z^2}+\\(d_{13}+d_{66})\frac{\partial^2 w_s}{\partial r\partial z}\end{bmatrix}-(1+\tau_\varepsilon^\alpha D^\alpha)\begin{bmatrix}n^s\frac{\partial p^f}{\partial r}+\rho^s\frac{\partial^2 u_s}{\partial t^2}-\\S_r(\frac{\partial u_f}{\partial t}-\frac{\partial u_s}{\partial t})\end{bmatrix}=0 \tag{4a}$$

$$(1+\tau_\sigma^\alpha D^\alpha)\begin{bmatrix}(d_{66}+d_{13})(\frac{\partial^2 u_s}{\partial r\partial z}+\frac{1}{r}\frac{\partial u_s}{\partial z})+\\d_{66}(\frac{\partial^2 w_s}{\partial r^2}+\frac{1}{r}\frac{\partial w_s}{\partial r})+d_{33}\frac{\partial^2 w_s}{\partial z^2}\end{bmatrix}-(1+\tau_\varepsilon^\alpha D^\alpha)\begin{bmatrix}n^s\frac{\partial p^f}{\partial z}+\rho^s\frac{\partial^2 w_s}{\partial t^2}-\\S_z(\frac{\partial w_f}{\partial t}-\frac{\partial w_s}{\partial t})\end{bmatrix}=0 \tag{4b}$$

$$n^f\frac{\partial p^f}{\partial r}+\rho^f\frac{\partial^2 u_f}{\partial t^2}+S_r(\frac{\partial u_f}{\partial t}-\frac{\partial u_s}{\partial t})=0 \tag{4c}$$

$$n^f\frac{\partial p^f}{\partial z}+\rho^f\frac{\partial^2 w_f}{\partial t^2}+S_z(\frac{\partial w_f}{\partial t}-\frac{\partial w_s}{\partial t})=0 \tag{4d}$$

$$\frac{\partial}{\partial r}(n^s\frac{\partial u_s}{\partial t}+n^f\frac{\partial u_f}{\partial t})+\frac{1}{r}(n^s\frac{\partial u_s}{\partial t}+n^f\frac{\partial u_f}{\partial t})+\frac{\partial}{\partial z}(n^s\frac{\partial w_s}{\partial t}+n^f\frac{\partial w_f}{\partial t})=0 \tag{4e}$$

Where u_s and u_f are respectively the radial displacement components for the soil skeleton and the pore fluid, while w_s and w_f their vertical displacement components; $S_r=\dfrac{(n^f)^2\gamma^f}{k_r^f}$ and $S_z=\dfrac{(n^f)^2\gamma^f}{k_z^f}$, of which γ^f represents the fluid weight per unit volume, and k_r^f and k_z^f are respectively the Darcy's permeability coefficients at the *r* and *z* directions.

Note that by setting $E_{vs}=E_{hs}$, $\upsilon_{vhs}=\upsilon_{hhs}$, and $\tau_\sigma=\tau_\varepsilon$, Eq. (4) can be reducible to the isotropic porous medium model built from Boer and Liu (1994).

As depicted in Fig. 1, with consideration of the viscosity and the transverse inertia effect for the embedded pile, which is treated as a Rayleigh-Love rod, its equation of motion can be built as

$$E_p\pi r_0^2\frac{\partial^2 w_p}{\partial z^2}+\pi r_0^2\eta_p\frac{\partial^3 w_p}{\partial z^2\partial t}-\rho_p\pi r_0^2\left[\frac{\partial^2 w_p}{\partial t^2}-\frac{1}{2}\upsilon_p^2 r_0^2\frac{\partial^4 w_p}{\partial z^2\partial t^2}\right]+f_s=0 \tag{5}$$

and the pile axial force can be written by

$$N_p(z)=E_p\pi r_0^2\frac{\partial w_p}{\partial z}+\pi r_0^2\eta_p\frac{\partial^2 w_p}{\partial z\partial t}+\frac{1}{2}\rho_p\pi r_0^2\upsilon_p^2 r_0^2\frac{\partial^3 w_p}{\partial z\partial t^2} \tag{6}$$

where w_p, E_p, η_p, ρ_p and υ_p respectively denote the vertical displacement, elastic modulus, damping coefficient, density and Poisson's ratio of the pile. The symbol f_s denotes the soil reaction on the side surface of the pile.

2.2 Boundary and continuity conditions for the soil and the pile

The pile-soil system considered satisfies the following boundary and continuity conditions:

The field variables decay to zero at infinity, i.e.

$$w_s(r\to\infty,z,t)=0 \tag{7a}$$

The soil top surface at $r>r_0$ is free of tractions and pervious, i.e.

$$\sigma_{zz}(r>r_0,z=0,t)=0,\quad p^f(r>r_0,z=0,t)=0 \tag{7b}$$

The underlying base is rigid and impermeable, i.e.

$$w_s(r,z=L,t)=w_f(r,z=L,t)=0 \tag{7c}$$

The pile-soil displacements at the interfaces are continuous, i.e.

$$w_s(r=r_0,z,t)=w_p(z,t) \tag{7d}$$

The axial force magnitude at the pile head equals to that for the applied loading, i.e.

$$N_p(z=0,t)=-p(t) \tag{7e}$$

The pile vertical displacement on the rigid base vanishes, i.e.

$$w_p(z=L,t)=0 \tag{7f}$$

2.3 Soil reaction f_s on the pile side surface

Here the soil reaction f_s is going to be obtained by solving Eq. (4) and then used in Eq. (5) for further derivation. Eq. (4(a)) through (4€) is actually very complicated and difficult to be analytically solved. Since

Nogami and Novak (1976), Novak (1977), Cai *et al*. (2009), Cai and Hu (2010) have shown that the influences of the soil radial displacement on the vertical vibration for pile-soil systems are negligible, this paper neglects the soil radial displacement and only considers the soil vertical propagation effect. Then Eq. (4(a)) through (4(e)) can be thus simplified as

$$(1+\tau_\sigma^\alpha \mathrm{i}^\alpha\omega^\alpha)\left[d_{66}(\frac{\partial^2 w_s}{\partial r^2}+\frac{1}{r}\frac{\partial w_s}{\partial r})+d_{33}\frac{\partial^2 w_s}{\partial z^2}\right]-(1+\tau_\varepsilon^\alpha \mathrm{i}^\alpha\omega^\alpha)\left[\frac{\partial p^f}{\partial z}-\rho^s\omega^2 w_s-\rho^f\omega^2 w_f\right]=0 \tag{8a}$$

$$n^f\frac{\partial p^f}{\partial z}-\rho^f\omega^2 w_f+\mathrm{i}\omega S_z(w_f-w_s)=0 \tag{8b}$$

$$\frac{\partial}{\partial z}(n^s w_s+n^f w_f)=0 \tag{8c}$$

where the time term of $\mathrm{e}^{\mathrm{i}\omega t}$ is omitted for brevity.

The combination of Eq. (8(a)) with Eq. (8(b)) leads to

$$\delta(\frac{\partial^2 w_s}{\partial r^2}+\frac{1}{r}\frac{\partial w_s}{\partial r})+\frac{\partial^2 w_s}{\partial z^2}-D_2 w_f-D_3 w_s=0 \tag{9}$$

where $\delta=\dfrac{G_{vs}(1-\upsilon_{hhs}-2\upsilon_{hvs}\upsilon_{vhs})}{E_{vs}(1-\upsilon_{hhs})}$, $D_1=\dfrac{1+\tau_\varepsilon^\alpha \mathrm{i}^\alpha\omega^\alpha}{1+\tau_\sigma^\alpha \mathrm{i}^\alpha\omega^\alpha}$, $D_2=\dfrac{D_1(n^s\rho^f\omega^2-\mathrm{i}\omega S_z)}{d_{33}n^f}$, and $D_3=\dfrac{D_1}{d_{33}}(\dfrac{\mathrm{i}\omega S_z}{n^f}-\rho^s\omega^2)$

It is obtained from Eq. (8(c)) that

$$\frac{\partial w_f}{\partial z}=-\frac{n^s}{n^f}\frac{\partial w_s}{\partial z} \tag{10}$$

By setting $\overline{w}_f=\dfrac{\partial w_f}{\partial z}$ and $\overline{w}_s=\dfrac{\partial w_s}{\partial z}$, Eq. (9) can be rewritten as

$$\delta(\frac{\partial^2 \overline{w}_s}{\partial r^2}+\frac{1}{r}\frac{\partial \overline{w}_s}{\partial r})+(\frac{D_2 n^s}{n^f}-D_3)\overline{w}_s+\frac{\partial^2 \overline{w}_s}{\partial z^2}-=0 \tag{11}$$

Assuming $\overline{w}_s=R(r)Z(z)$, then inserting this variable into Eq. (11) yields

$$\frac{\partial^2 R(r)}{\partial r^2}+\frac{1}{r}\frac{\partial R(r)}{\partial r}-q^2R(r)=0 \tag{12a}$$

$$\frac{\partial^2 Z(z)}{\partial z^2}-g^2Z(z)=0 \tag{12b}$$

where $\delta q^2+g^2=D_3-\dfrac{D_2 n^s}{n^f}$, $Re(q)>0$, and $Re(g)>0$.

The solutions for Eqs. (12(a) and 12(b)) can be found to be

$$R(r)=AK_0(qr)+BI_0(qr) \tag{13a}$$

$$Z(z)=C\mathrm{e}^{gz}+D\mathrm{e}^{-gz} \tag{13b}$$

where *A*, *B*, *C*, and *D* are unknown constants. $I_0(\cdot)$ and $K_0(\cdot)$ are respectively the 0-order modified Bessel's functions of the first and second kinds.

It is then obtained from Eqs. (2(c)), (7(a)) and (7(b)) that

$$w_s=A_1\frac{K_0(qr)}{g}(\mathrm{e}^{gz}+\mathrm{e}^{-gz}) \tag{14}$$

where $A_1=AC$.

Substituting Eq. (14) into Eq. (7(c)) results in an eigenvalue which is given by

$$g=a_n=\frac{(2n-1)\pi\mathrm{i}}{2L} \tag{15}$$

where $n=1,\ 2,\ 3\cdots\infty$.

Then w_s can be written as

$$w_s=\sum_{n=1}^{\infty}\frac{A_n}{a_n}K_0(q_n r)(\mathrm{e}^{a_n z}+\mathrm{e}^{-a_n z}) \tag{16}$$

By combining Eqs. (2(d)) and (16), the shear stress of the soil is obtained as

$$\tau_{zr}=\frac{d_{66}}{D_1}\frac{\partial w_s}{\partial r}=-\frac{d_{66}}{D_1}\sum_{n=1}^{\infty}\frac{A_n q_n}{a_n}K_1(q_n r)(\mathrm{e}^{a_n z}+\mathrm{e}^{-a_n z}) \tag{17}$$

The soil reaction of f_s at the side surface for the pile is thus derived as

$$f_s(z)=2\pi r_0\tau_{zr}(r=r_0,z)=-2\pi r_0\frac{d_{66}}{D_1}\sum_{n=1}^{\infty}\frac{A_n q_n}{a_n}K_1(q_n r_0)(\mathrm{e}^{a_n z}+\mathrm{e}^{-a_n z}) \tag{18}$$

Here A_n is still unknown and will be determined with the pile-soil continuity conditions.

2.4 Pile's displacement, axial force, and dynamic impedance in frequency domain

Eq. (5) can be further deduced as

$$\frac{\partial^2 w_p}{\partial z^2}+\lambda^2 w_p=\frac{2d_{66}\lambda^2}{D_1 r_0\rho_p\omega^2}\sum_{n=1}^{\infty}A_n\frac{q_n K_1(q_n r_0)}{a_n}(\mathrm{e}^{a_n z}+\mathrm{e}^{-a_n z}) \tag{19}$$

where $\lambda^2=\dfrac{\rho_p\omega^2}{E_p+\mathrm{i}\omega\eta_p-\frac{1}{2}\upsilon_p^2 r_0^2\rho_p\omega^2}$ and $Re(\lambda)>0$.

The solution of Eq. (19) is

$$w_p=a_1\cos(\lambda z)+a_2\sin(\lambda z)+\sum_{n=1}^{\infty}A_n Q_n(\mathrm{e}^{a_n z}+\mathrm{e}^{-a_n z}) \tag{20}$$

where $Q_n=\dfrac{2d_{66}\lambda^2 q_n K_1(q_n r_0)}{D_1 r_0\rho_p\omega^2 a_n(a_n^2+\lambda^2)}$, and a_1 and a_2 are undetermined coefficients.

Substituting Eq. (16) and (20) into the pile-soil continuity formula (7d) yields

$$a_1\cos(\lambda z)+a_2\sin(\lambda z)+\sum_{n=1}^{\infty}A_n Q_n(\mathrm{e}^{a_n z}+\mathrm{e}^{-a_n z})=\sum_{n=1}^{\infty}A_n\frac{K_0(q_n r_0)}{a_n}(\mathrm{e}^{a_n z}+\mathrm{e}^{-a_n z}) \tag{21}$$

With the orthogonality of the functions $(\mathrm{e}^{a_n z}+\mathrm{e}^{-a_n z})$ at $[0,L]$, which is given by

$$\int_0^L(\mathrm{e}^{a_n z}+\mathrm{e}^{-a_n z})(\mathrm{e}^{a_m z}+\mathrm{e}^{-a_m z})\mathrm{d}z=\begin{cases}0, m\neq n\\ 2L, m=n\end{cases} \tag{22}$$

it is determined from Eq. (21) that

$$A_n=X_{1n}a_1+X_{2n}a_2 \tag{23}$$

where $X_{1n}=\dfrac{\int_0^L \cos(\lambda z)(\mathrm{e}^{a_n z}+\mathrm{e}^{-a_n z})\mathrm{d}z}{2L\left[\dfrac{K_0(q_n r_0)}{a_n}-Q_n\right]}$

$$X_{2n}=\frac{\int_0^L \sin(\lambda z)(\mathrm{e}^{a_n z}+\mathrm{e}^{-a_n z})\mathrm{d}z}{2L\left[\dfrac{K_0(q_n r_0)}{a_n}-Q_n\right]}$$

Eq. (20) can thus be rewritten by

$$w_p=a_1\left[\cos(\lambda z)+\sum_{n=1}^{\infty}Q_n X_{1n}(\mathrm{e}^{a_n z}+\mathrm{e}^{-a_n z})\right]+a_2\left[\sin(\lambda z)+\sum_{n=1}^{\infty}Q_n X_{2n}(\mathrm{e}^{a_n z}+\mathrm{e}^{-a_n z})\right] \quad (24)$$

From Eq. (6), the pile axial force can be obtained as

$$N_p(z)=\pi r_0^2(E_p+\mathrm{i}\omega\eta_p-\frac{1}{2}\upsilon_p^2 r_0^2\rho_p\omega^2)\left\{\begin{array}{l}a_1\left[-\lambda\sin(\lambda z)+\sum_{n=1}^{\infty}Q_n X_{1n}a_n(\mathrm{e}^{a_n z}-\mathrm{e}^{-a_n z})\right]+\\ a_2\left[\lambda\cos(\lambda z)+\sum_{n=1}^{\infty}Q_n X_{2n}a_n(\mathrm{e}^{a_n z}-\mathrm{e}^{-a_n z})\right]\end{array}\right\} \quad (25)$$

The insertion of Eqs. (24) and (25) into the boundary conditions of Eqs. (7(e)) and (7(f)) produces

$$a_2=\frac{\tilde{p}}{\pi r_0^2\lambda(E_p+\mathrm{i}\omega\eta_p-\frac{1}{2}\upsilon_p^2 r_0^2\rho_p\omega^2)},\quad a_1=-\frac{X_2}{X_1}a_2 \quad (26)$$

where $X_1=\cos(\lambda L)+\sum_{n=1}^{\infty}Q_n X_{1n}(\mathrm{e}^{a_n L}+\mathrm{e}^{-a_n L})$ and

$X_2=\sin(\lambda L)+\sum_{n=1}^{\infty}Q_n X_{2n}(\mathrm{e}^{a_n L}+\mathrm{e}^{-a_n L})$ ·

It is meaningful to define the impedance function for the pile head by

$$K_d=K_R+\mathrm{i}C_I=\frac{p(t)}{w_p(z=0)}=\frac{\tilde{p}}{a_1(1+2\sum_{n=1}^{\infty}Q_n X_{1n})+2a_2\sum_{n=1}^{\infty}Q_n X_{2n}} \quad (27)$$

where $K_R=real(K_d)$ denotes the realistic dynamic stiffness representing the capacity resisting the axial strain of the pile-soil system, while $C_I=imag(K_d)$ the equivalent damping generated from the wave radiation effects and material damping of the pile-soil system, and the relative motion for the soil skeleton and the pore fluid, which reflects the energy dissipative property for the pile-soil system.

Therefore, the dynamic impedance for the pile top can be used for estimating the vibration property and bearing capacity for pile-soil systems, which can be taken as the impedance input at the bottom of superstructures in the separation designs with substructure methods.

2.5 Time-domain velocity response at the pile head

The integrity test of pile foundations under low strain conditions is usually performed by striking the pile top with a hammer and then monitoring the velocity response curve of the pile top. Then the hammering excitation is generally simplified to the half sine impulse load in the form of

$$q(t)=\begin{cases}Q_{\max}\sin\dfrac{\pi t}{T} & 0\le t\le T\\ 0 & t>T\end{cases} \quad (28)$$

where $Q_{\max}$ is the impulse magnitude and T the impulse width, as shown in Fig. 2.

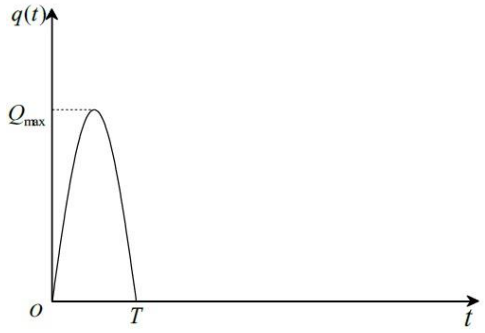

Fig. 2 A half-sine exciting force

Furthermore, by combining Eqs. (24) and (27), the frequency-domain velocity response for the pile top under an unit load can be obtained as

$$\tilde{V}(\omega)=\frac{\mathrm{i}\omega}{K_d(\omega)} \quad (29)$$

Then the time-domain velocity response of the pile head can be derived by the convolution for the applied load of $q(t)$ and the inverse Fourier transform of $\tilde{V}(\omega)$, which is given by

$$V(t)=\frac{1}{2\pi}\int_{-\infty}^{+\infty}\frac{\mathrm{i}\omega}{K_d(\omega)}Q_{\max}\frac{\pi}{T}\frac{1+\mathrm{e}^{-\mathrm{i}\omega T}}{(\frac{\pi}{T})^2-\omega^2}\mathrm{e}^{\mathrm{i}\omega t}\mathrm{d}\omega \quad (30)$$

In the nondestructive testing for pile foundations, this velocity response for the pile top by hammering is generally used to evaluate the speed of stress waves, examine the field test data, and find the defects in piles.

3. Numerical results and discussions

This section performs the numerical computation of examples for the accuracy validation of the proposed solutions and the dynamic property study for the pile soil system. Unless otherwise stated, the material parameter values for the pile soil system are listed in Table 1. Also, taking the applied force amplitude of $\widetilde{p}=1231.25$ KN for the steady- state vibration analysis. While for the transient response analysis of the pile integrity test, considering the impulse force with $Q_{\max}=1304$ N and T=2 ms excited from polythene hammers.

3.1 Verification of the solution

Three comparisons below are performed to verify the present solutions.

Case 1: Given $E_{vs}=E_{hs}$ and $\upsilon_{vhs}=\upsilon_{hhs}$, the present solution is reduced to an isotropic saturated soil solution and compared with the impedance function results for the pile top by Liu *et al*. (2014), as plotted in Fig. 3. Note that for the comparison, Liu *et al*. (2014)'s solution, which is derived for pipe piles, has been reduced to a solid pile solution by setting its inner radius to zero.

Case 2: Setting $\rho^{fR}\to 0$ and $n^f\to 0$, the presented solution is reducible to a transversely isotropic single-phase

Table 1 Material parameters for the pile-soil system

Models	Parameters	Symbols	Values	Units
Pile	Length	L	10	m
	Radius	r_0	0.25	m
	Young's modulus	E_p	20	GPa
	Density	ρ_p	2500	kg/m^3
	Damping coefficient	η_p	1×10^5	Pa·s
	Poisson's ratio	υ_p	0.1	-
Soil	Parameters of the transversely isotropic model	E_{hs}	38	MPa
		E_{vs}	50	MPa
		υ_{vhs}	0.21	-
		υ_{hhs}	0.12	-
		G_{vs}	19.7	MPa
	True density of soil skeleton	ρ^{sR}	1818	kg/m^3
	True density of pore fluid	ρ^{fR}	1000	kg/m^3
	Volume fraction of pore fluid	n^f	0.37	-
	Darcy's coefficients of permeability	k^f	1.6	mm/s
	Parameters of the fractional derivative model	α	0.4	-
		τ_σ	1.6×10^5	s
		τ_ε	1.2×10^5	s

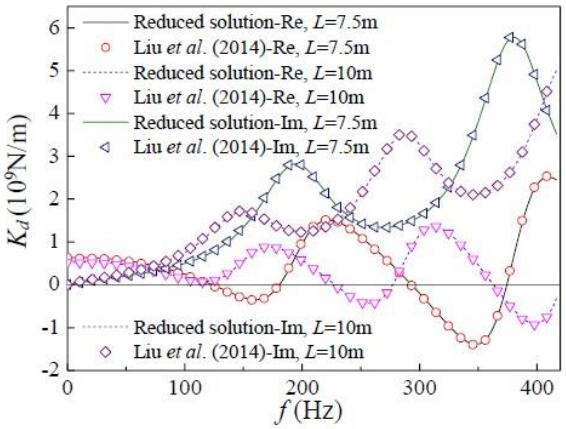

Fig. 3 The present reduced solution versus Liu *et al*. (2014)'s solution for the isotropic saturated soil

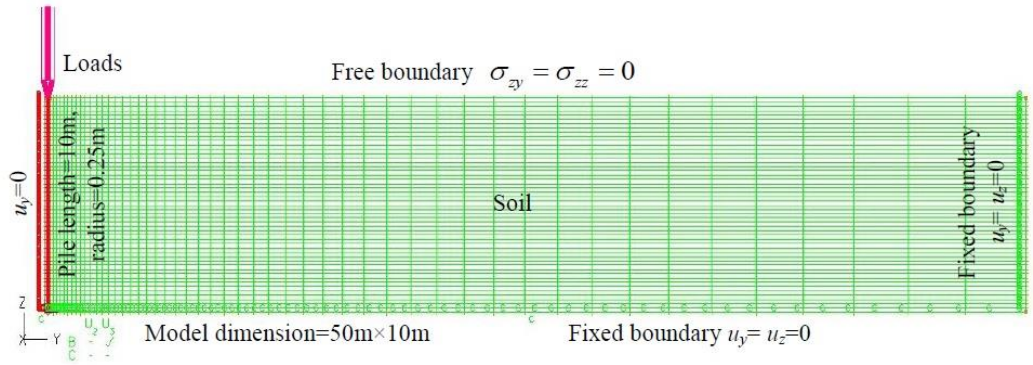

Fig. 4 Axisymmetric pile-soil FE model established by the ADINA software

soil solution and compared with the FEM (ADINA) results of the displacement and velocity responses of Figs. 4 and 5. It is noted that in the FE model, using the above-mentioned parameters values for the pile-soil materials and the applied loads, and taking the excitation frequency of $f=16.6\,\mathrm{Hz}$ for the time-harmonic load case; the pile and soil models

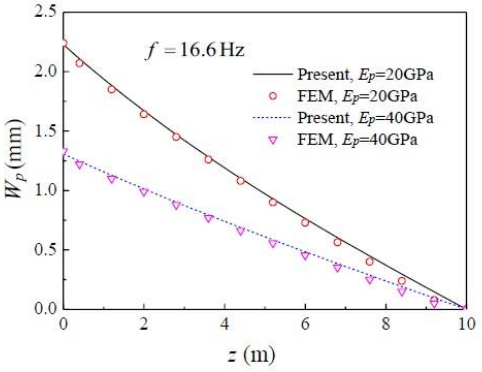

(a) Pile shaft displacement

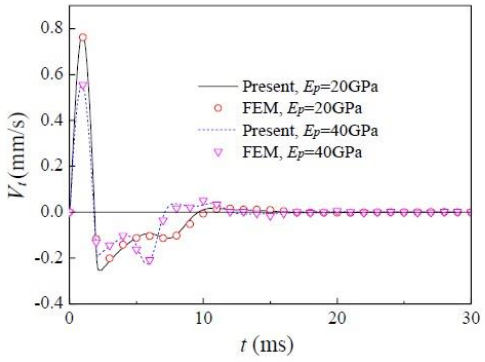

(b) Pile top velocity

Fig. 5 The present reduced results versus the FEM (ADINA) results for the single-phase transversely isotropic soil

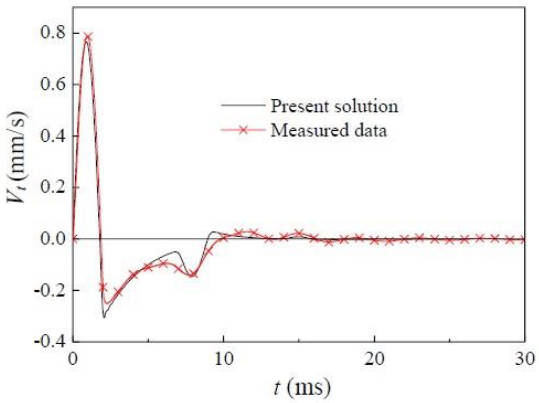

Fig. 6 The present result versus the measured velocity data in the pile field test

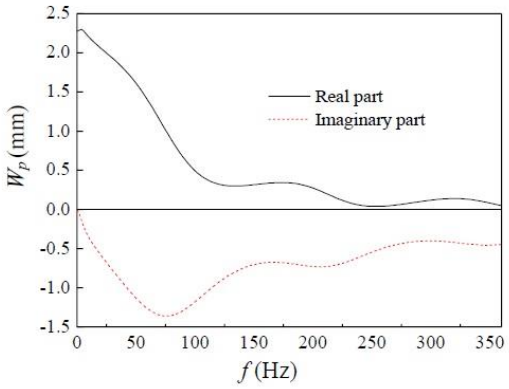

Fig. 7 The displacement of the pile head against the excitation frequency.

are meshed by the number of subdivisions and the length ratio of element edges (last/first). And the two meshing parameters of 50 and 1 used for the vertical edges of the pile and soil regions, 4 and 1 for the horizontal edges of the pile region, while 50 and 20 for the horizontal edges of the soil region; the 9-node high-order rectangle elements with the linearly-elastic isotropic/transversely isotropic constitutive laws are used to simulate the pile and the soil,respectively, and the pile-soil element nodes at their contact boundaries are in coincidence; the boundary condition setting for the pile-soil system is pictured in Fig. 4; the model horizontal length of 50m is enough to remove the boundary effects from the fixed boundary setting at the model right-hand side. The FE model is corresponding to the pile-soil model of Fig. 1.

Case 3: Fig. 6 shows that the presented solution is compared to the pile head velocity data measured in the pile field testing in Dalian harbor. Note that the pile-soil material parameters obtained in the pile testing field have been listed in Table 1. It is observed from these comparisons that they agree well, and the curve endpoints are consistent with the pile-soil boundary conditions as well. The present solutions are thus validated.

3.2 Parametric analyses of the pile-soil dynamic responses

The pile-soil dynamic responses are dependent on many factors (e.g., the applied loads and the pile-soil parameters). As the effects of these parameters (e.g., the pile's length, the pile-soil modulus ratio, and the soil's permeability coefficient, etc) have been discussed in other studies, present attention is paid to study the influence of the transversely isotropic parameter of δ and the excitation frequency of f. It should be noted that by δ's definition, one can see δ is the combination of those five independent transversely isotropic parameters, such that the influence of the soil anisotropy on the pile-soil system under consideration can be directly reflected by δ's variation.

Figs. 7 and 8 show the effect of the excitation frequency on the pile displacement. As can be found from these plots, with the increasing excitation frequency the displacement of the pile head fluctuates and decreases as a whole, which reflects the resonant behavior and deformation characteristic of the pile-soil system. The effect of the excitation frequency on the pile axial force is plotted in Fig. 9. One can see that against the increase of the excitation frequency, the axial force curve for the pile shaft also fluctuates and the pile generates tension. This is because the increase of the excitation frequency means the vibration energy of the pile-soil system increases, resulting in the pile-soil interaction and wave propagations enhanced.

Fig. 10 shows the influence of the soil anisotropy on the

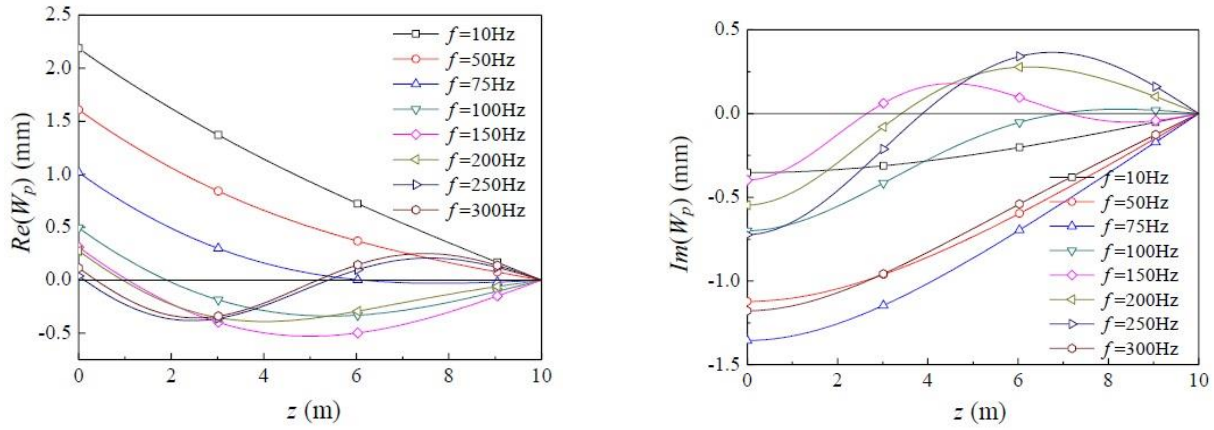

Fig. 8 The pile shaft displacement distributions under different excitation frequencies

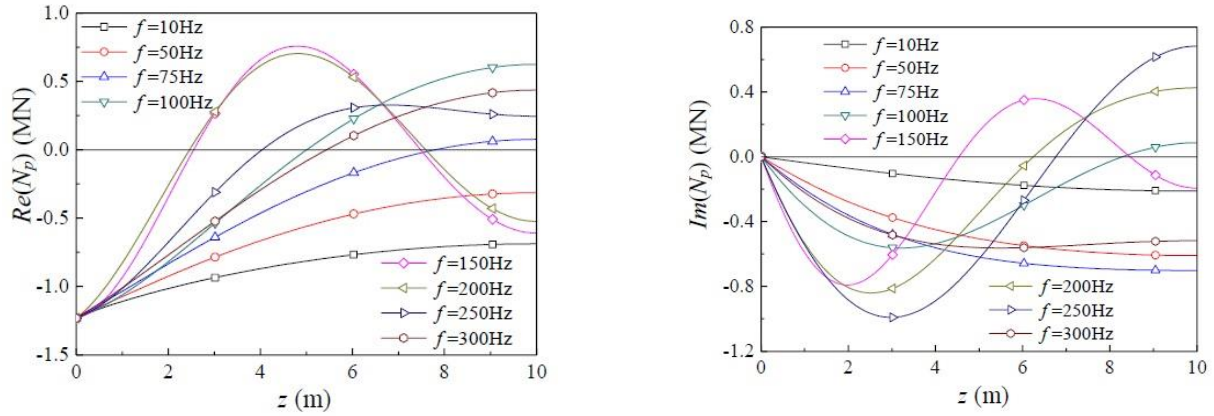

Fig. 9 The axial force distributions of the pile shaft under different excitation frequencies

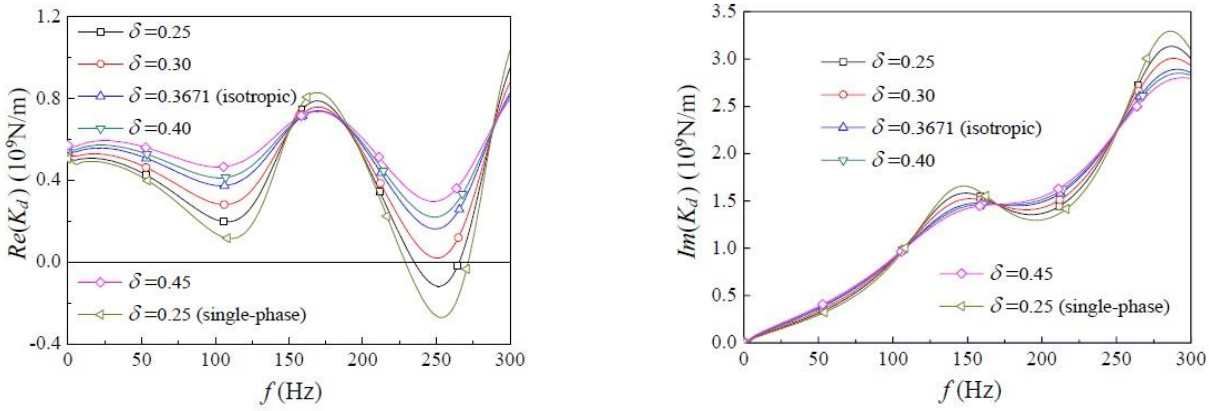

Fig. 10 Influence of the transverse-isotropic parameter of δ on the pile head impedance function

pile top impedance function. It is found that as the transversely isotropic parameter of δ increases, which may mean the vertical shearing modulus of the soil increases and then the pile-soil system becomes more stiff, the static pile top stiffness increases while the fluctuation amplitudes of the dynamic impedance curves for the pile top decrease. Also, compared to the real part (stiffness) of the impedance function, its imaginary part (damping) is less sensitive to the change of δ.

Fig. 11 indicates the influence of the soil anisotropy on the pile shaft displacement. It can be seen that at the low excitation frequency, the pile shaft displacement decreases as δ increases; at the high excitation frequency, with the increase of δ the extreme value of the real part for the pile shaft displacement decreases, while the imaginary part of the pile shaft displacement shows negligible change except for the obvious increase at the pile head. Similar changes also can be found in Fig. 12 that reveals the

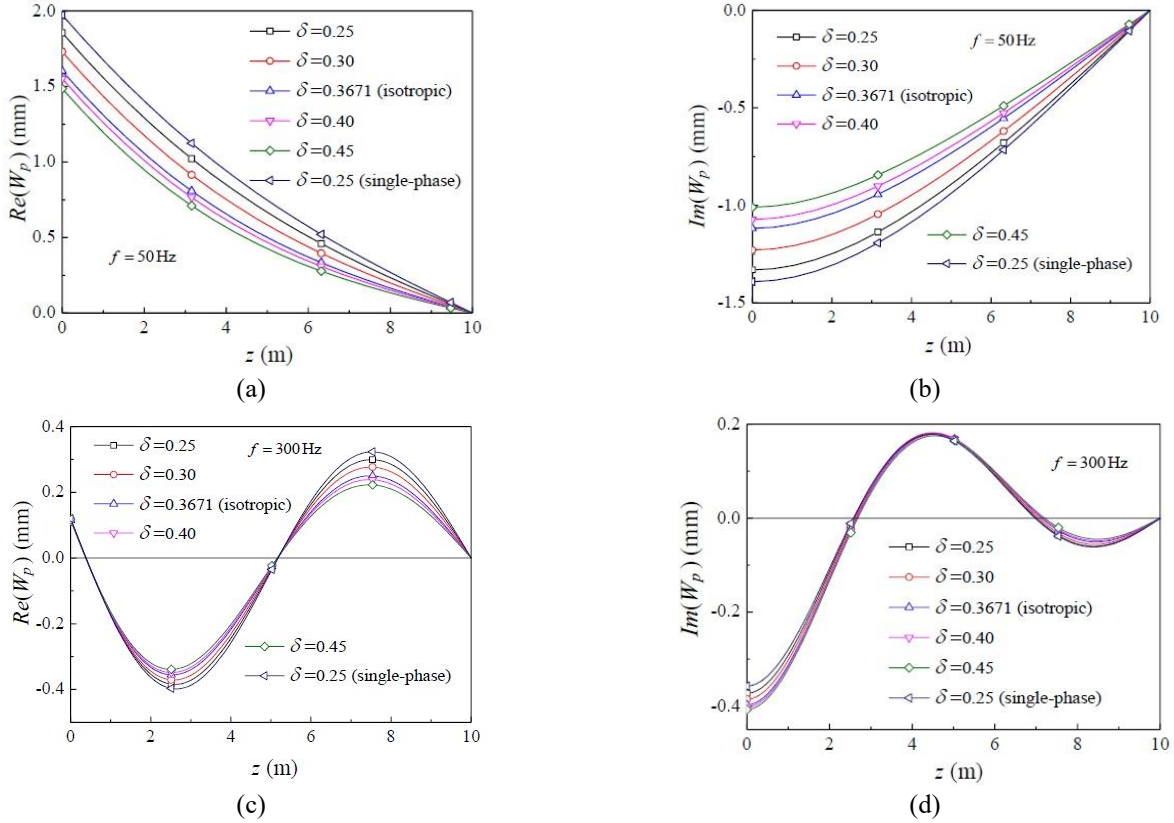

Fig. 11 Influence of the transverse-isotropic parameter of δ on the pile shaft displacement

influence of the soil anisotropy on the pile shaft axial force. As explained in the above, these variations are basically corresponding to those of the dynamic impedance in Fig. 10.

The influence of the soil anisotropy on the pile top velocity is plotted as Fig. 13. It can be observed that with the increase of δ, the reflection signal magnitudes for the pile decrease, but the reflection positions are almost unchanged. This implies that within the range of δ under consideration, the reflection positions of the impulse excitation mainly depend on the actual pile length. Therefore, for the integrity testing of piles, the soil anisotropy can be negligible as long as the reflection signal amplitude can be identified. Also, the comparisons of the single-phase and saturated soil cases in Figs. 10-13 confirm that the pore liquid has noticeable effects on the pile-soil dynamic property.

4. Conclusions

In this paper, the dynamic analyses for an axially loaded pile buried in a transverse-isotropic, fluid-saturated, poro-visco-elastic soil underlain by rigid base has been done with analytical investigation. Meanwhile the analytical solutions for the impedance function, the displacement and the axial force of the pile in the frequency domain, and the time-domain velocity response at the pile top are presented. By the comparisons with the reported solution, the FEM results, and the field testing data, the proposed solutions are verified. As illustrations, results for the influence of the soil anisotropy and the excitation frequency on the pile-soil system are also included. Some significant conclusions can be drawn as follows:

- For the soil underlain by rigid base, there exists significant resonant behavior. Against the increasing excitation frequency, the pile-soil dynamic responses fluctuate, and the impedance function of the pile top increases as a whole.
- The soil anisotropy has noticeable influences on the dynamic responses of the pile-soil system, especially for the frequency-domain response analyses. While for the integrity testing of piles, with the varying transverse-isotropic parameter the reflected positions of impulse excitations basically keep unchanged and then the soil anisotropy can be negligible.
- From the comparison results for the reduced and existing solutions, the present solutions can cover some classical solutions, which provide a wide variety of application for related engineering designs and practices.

Acknowledgements

This work is supported by the National Natural Science Foundation of China [Grant number 51908070, 51978085, 51927814, and 52025085], the Natural Science Foundation of Hunan Province (2020JJ5596), the Excellent Youth

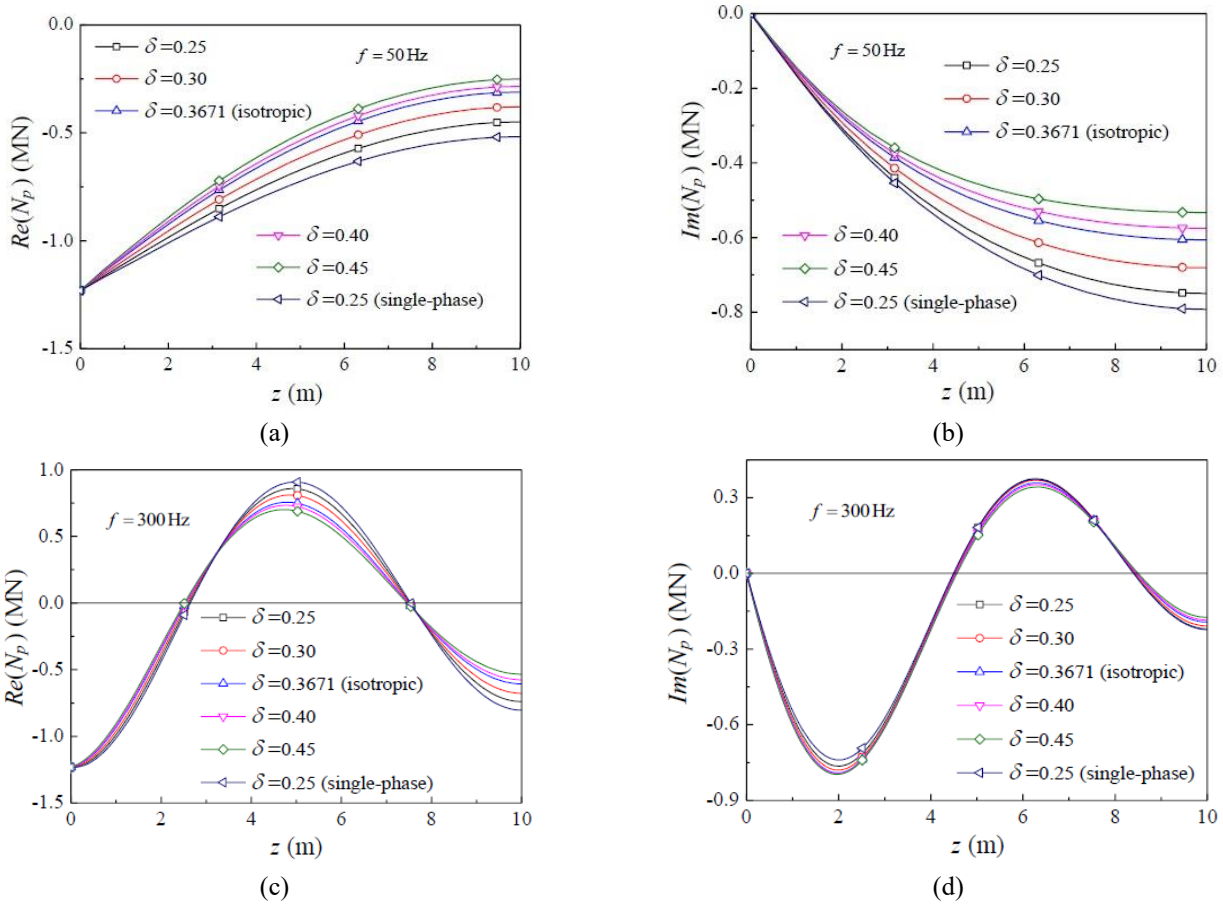

Fig. 12 Influence of the transverse-isotropic parameter of δ on the pile shaft axial force

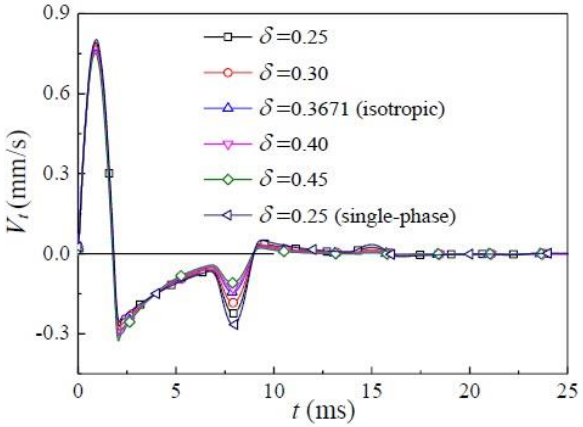

Fig. 13 Influence of the transverse-isotropic parameter of δ on the pile top velocity

Foundation of Natural Science Foundation of Hunan Province (2018JJ1026), the Key Project of Education Department of Hunan Province (17A008), the Training Program for High-level Technical Personnel in Transportation Industry (2018-025), the Open Funds of the National Engineering Laboratory of Highway Maintenance Technology through Grant kfj190103, and the Key Laboratory of Road Structure and Material of the Ministry of Transport through Grant kfj170304 (Changsha University of Science & Technology).

References

Ai, Z.Y. and Li, Z.X. (2015), "Dynamic analysis of a laterally loaded pile in a transversely isotropic multilayered half-space", *Eng. Anal. Bound. Elem.*, **54**, 68-75. https://doi.org/10.1016/j.enganabound.2015.01.008.

Ai, Z.Y. and Liu, C.L. (2015), "Vertical vibration of a pile in transversely isotropic multilayered soils", *J. Sound Vib.*, **357**, 145-155. https://doi.org/10.1016/j.jsv.2015.07.032.

Ai, Z.Y., Li, Z.X. and Wang, L.H. (2016), "Dynamic response of a laterally loaded fixed-head pile group in a transversely isotropic multilayered half-space", *J. Sound Vib.*, **385**, 171-183. https://doi.org/10.1016/j.jsv.2016.09.016.

Ai, Z.Y., Liu, C.L. and Wang, L.J. (2016), "Vertical vibration of a partially embedded pile group in transversely isotropic soils", *Comput. Geotech.*, **80**, 107-114. https://doi.org/10.1016/j.compgeo.2016.06.017.

Bagley, R.L. and Torvik, P.J. (1983), "A theoretical basis for the application of fractional calculus to viscoelasticity", *J. Rheol.*, **27**(3), 201-210. https://doi.org/10.1122/1.549724.

Barari, A., Bayat, M. and Saadati, M. (2015), "Transient analysis of monopile foundations partially embedded in liquefied soil", *Geomech. Eng.*, **8**(2), 257–282. https://doi.org/10.12989/gae.2015.8.2.257.

Barros, P.L.A., Labaki, J. and Mesquita, E. (2019), "IBEM-FEM model of a piled plate within a transversely isotropic half-space", *Eng. Anal. Bound. Elem.*, **101**, 281-296. https://doi.org/10.1016/j.enganabound.2018.12.013.

Boer, D.R. and Liu, Z.F. (1994), "Plane waves in a semi-infinite fluid saturated porous medium", *Transport Porous Med.*, **16**,

147-173. https://doi.org/10.1007/BF00617549.

Cai, Y.Q. and Hu, X.Q. (2010), "Vertical Vibrations of a rigid foundation embedded in a poroelastic half-space", *J. Eng. Mech*., **136**, 390-398. https://doi.org/10.1061/(ASCE)0733-9399(2010)136:3(390).

Cai, Y.Q., Hu, X.Q. and Xu, C.J. (2009), "Vertical dynamic response of a rigid foundation embedded in a poroelastic soil layer", *Int. J. Numer. Anal. Met. Geomech*., **33**, 1363-1388. https://doi.org/10.1002/nag.766.

Chen, G., Cai, Y.Q. and Liu, F.Y. (2008), "Dynamic response of a pile in a transversely isotropic saturated soil to transient torsional loading", *Comput. Geotech*., **35**, 165-172. https://doi.org/10.1016/j.compgeo.2007.05.009.

Cui, C.Y., Zhang, S.P. and Chapman, D. (2018), "Dynamic impedance of a floating pile embedded in poro-visco-elastic soils subjected to vertical harmonic loads", *Geomech*. *Eng*., **15**(2), 793-803. https://doi.org/10.12989/gae.2018.15.2.793.

Gharahi, A., Rahimian, M. and Eskandari-Ghadi, M. (2014), "Dynamic interaction of a pile with a transversely isotropic elastic half-space under transverse excitations", *Int. J. Solids Struct*., **51**, 4082-4093. https://doi.org/10.1016/j.ijsolstr.2014.08.001.

Liu, H.L., Zheng, C.J. and Ding, X.M. (2014), "Vertical dynamic response of a pipe pile in saturated soil layer", *Comput. Geotech*., **61**, 57–66. https://doi.org/10.1016/j.compgeo.2014.04.006.

Miller, K.S. and Ross, B. (1993), An Introduction to the Fractional Calculus and Fractional Differential Equations, Wiley, New York, NY, USA.

Nogami, T. and Novak, M. (1976), "Soil-pile interaction in vertical vibration", *Earthq. Eng. Struct. D.*, **4**(3), 277-293. https://doi.org/10.1002/eqe.4290040308.

Novak, M. (1977), "Vertical vibration of floating piles", *J. Eng. Mech*., **103**(1), 153-168.

Shahbodagh, B., Ashari, M. and Khalili, N. (2017), "A hybrid element method for dynamics of piles and pile groups in transversely isotropic media", *Comput. Geotech*., **85**, 249-261. https://doi.org/10.1016/j.compgeo.2016.12.029.

Shahmohamadi, M., Khojasteh, A. and Rahimian, M. (2011a), "Axial soil-pile interaction in a transversely isotropic half-space", *Int. J. Eng. Sci*., **49**, 934-949. https://doi.org/10.1016/j.ijengsci.2011.05.004.

Shahmohamadi, M., Khojasteh, A. and Rahimian, M. (2011b), "Seismic response of an embedded pile in a transversely isotropic half-space under incident P-wave excitations", *Soil Dyn. Earthq. Eng*., **31**, 361-371. https://doi.org/10.1016/j.soildyn.2010.09.005.

Shahmohamadi, M., Khojasteh, A. and Rahimian, M. (2013), "Dynamics of a cylindrical pile in a transversely isotropic half-space under axial excitations", *J. Eng. Mech*., **139**(5), 568-579. https://doi.org/10.1061/(ASCE)EM.1943-7889.0000511.

Tajimi, H. (1969), "Dynamic analysis of a structure embedded in an elastic stratum", Proceedings of 4th World Conference on Earthquake Engineering, Santiago, Chile, January.

Wang, C.D. (2004), "Three-dimensional nonlinearly varying rectangular loads on a transversely isotropic half-space", *Int. J. Geomech*., **4**(4), 240-253. https://doi.org/10.1061/(ASCE)1532-3641(2004)4:4(240).

Wang, C.D. and Liao, J.J. (2001), "Elastic solutions for a transversely isotropic half-space subjected to arbitrarily shaped loads using triangulating technique", *Int. J. Geomech*., **1**(2), 193-224. https://doi.org/10.1061/(ASCE)1532-3641(2001)1:2(193).

Wang, K.H., Zhang, Z.Q. and Leo, C.J. (2009), "Dynamic torsional response of an end bearing pile in transversely isotropic saturated soil", *J. Sound Vib*., **327**, 440-453. https://doi.org/10.1016/j.jsv.2009.06.017.

Zhang, S.P., Cui, C.Y. and Yang, G. (2019), "Vertical dynamic impedance of pile groups partially embedded in multilayered, transversely isotropic, saturated soils", *Soil Dyn. Earthq. Eng*., **117**, 106-115. https://doi.org/10.1016/j.soildyn.2018.11.003.

Zhang, S.P., Pak, Y.S.R. and Zhang, J.H. (2021), "Vertical time-harmonic coupling vibration of an impermeable, rigid, circular plate resting on a finite, poroelastic soil layer", *Acta Geotech*., 16, 911–935. https://doi.org/10.1007/s11440-020-01067-8.

Zhang, S.P., Pak, Y.S.R. and Zhang, J.H. (2022), "Three-dimensional frequency-domain Green's functions of a finite fluid-saturated soil layer underlain by rigid bedrock to interior loadings", *Int. J. Geomech*., **22**(1), 04021267. https://doi.org/10.1061/(ASCE)GM.1943-5622.0002235.

Zhang, S.P., Xu, Z. and Deng, C. (2022), "Vertical frequency-domain compliance of an elastic pipe pile embedded in a liquid-filled and porous-viscoelastic soil", *Int. J. Numer. Anal. Met. Geomech*., 1-25, https://doi.org/10.1002/nag.3347.

Zhang, S.P., Zhang, J.H., Ma, Y.B. and Pak Y.S.R. (2021), "Vertical dynamic interactions of poroelastic soils and embedded piles considering the effects of pile-soil radial deformations". *Soils Found.*, **61**, 16-34. https://doi.org/10.1016/j.sandf.2020.10.003.

Zheng, C.J., Hua, J.M. and Ding, X.M. (2016), "Torsional vibration of a pipe pile in transversely isotropic saturated soil", *Earthq. Eng. Eng. Vib*., **15**, 509-517. https://doi.org/10.1007/s11803-016-0340-2.

CC